ACS EARTH AND SPACE CHEMISTRY

Article

Cite This: ACS Earth Space Chem. XXXX, XXX, XXX−XXX

http://pubs.acs.org/journal/aesccq

HONO, Particulate Nitrite, and Snow Nitrite at a Midlatitude Urban Site during Wintertime

Qianjie Chen,[†] Jacinta Edebeli,[†,‡] Stephen M. McNamara,[†] Kathryn D. Kulju,[†] Nathaniel W. May,[†] Steven B. Bertman,[§] Sham Thanekar,[∥] Jose D. Fuentes,[∥] and Kerri A. Pratt*[,†,⊥]

[†]Department of Chemistry, University of Michigan, Ann Arbor, Michigan 48109, United States

[‡]Paul Scherrer Institut, 5232 Villigen, Switzerland

[§]Institute of the Environment and Sustainability, Western Michigan University, Kalamazoo, Michigan 49008, United States

[∥]Department of Meteorology and Atmospheric Science, Pennsylvania State University, University Park, Pennsylvania 16802, United States

[⊥]Department of Earth and Environmental Sciences, University of Michigan, Ann Arbor, Michigan 48109, United States

ABSTRACT: Nitrous acid (HONO) plays an important role in the oxidative capacity of the atmosphere during wintertime via photolysis to produce hydroxyl radicals (OH). While it is known that HONO is emitted from the Arctic snowpack, sparse observations of HONO in the midlatitude urban wintertime environment have hindered our understanding of cold-season atmospheric chemistry. In this study, measurements of ambient HONO, particulate nitrite (pN(III); N(III) = $NO_{2(aq)}^-$ + $HONO_{(aq)}$ + $H_2ONO_{(aq)}^+$), and snow nitrite (sN(III)) were conducted in Kalamazoo, Michigan during January−February 2018. Elevated levels of HONO and particulate nitrite were observed over snow-covered ground, likely due to emissions of HONO from the snowpack, as well as weak turbulent mixing in the atmospheric boundary layer. The noontime peak in HONO of 87 ± 60 (1σ) parts per trillion (ppt) over snow-covered ground suggests photochemical snowpack HONO production, likely in part through snowpack nitrate photolysis, with only a minor contribution from particulate nitrate photolysis. High concentrations of snow nitrite (0.4 ± 0.3 (1σ) μM) support the hypothesis that the snowpack is a significant source of HONO to the atmosphere. On average, the OH production rate from HONO photolysis, in the near-surface atmosphere (≈ 2 m above ground), was calculated to be about an order of magnitude higher than that from O_3 photolysis over snow-covered ground. Future studies are needed to quantify HONO emissions from the midlatitude urban snowpack, given expected HONO production due to high concentrations of snow nitrate and nitrite from anthropogenic particulate nitrate and nitrite deposition.

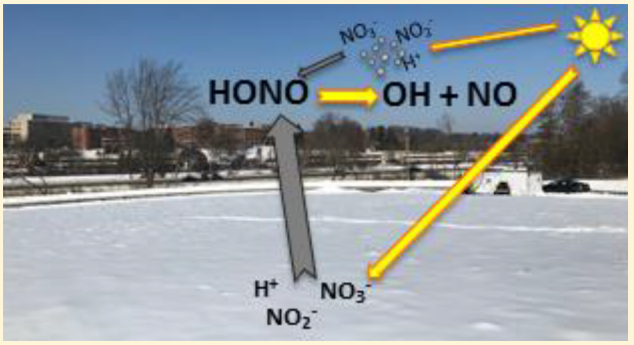

KEYWORDS: *HONO, nitrite, particle, snow, winter*

INTRODUCTION

Nitrous acid ($HONO_{(g)}$, denoted as HONO hereafter) is recognized as an important source of hydroxyl radicals (OH) in the troposphere, along with ozone (O_3) photolysis, formaldehyde (HCHO) photolysis, and alkene ozonolysis.[1−4] The production of OH and nitric oxide (NO) from photolysis of HONO further affects tropospheric chemistry, air quality, and climate via oxidation of methane and nonmethane hydrocarbons and formation of O_3 and peroxyacetyl nitrate (PAN).[5,6] Cloud and aerosol chemical composition are also altered through secondary organic aerosol formation, sulfate formation (via SO_2 + OH), and nitrate formation (via NO_2 + OH).[7,8] These impacts are especially amplified in polluted regions during winter when nitrogen oxides (NO_x = NO + NO_2) are abundant, and other photolytic OH sources are weak.[5,7,9,10] In particular, during wintertime, solar intensity is low, and water vapor abundance is reduced at low temperatures, making OH production from O_3 photolysis inefficient.[4] Yet, few studies have investigated the HONO budget in the midlatitude snowy wintertime environment.[11,12] Snow-covered ground is often associated with stable and shallow atmospheric boundary layers[13] and high surface albedo for solar radiation,[14] which affects the concentrations of trace gases and photochemical reactions (e.g., HONO photolysis) in the atmosphere. In addition, the snowpack can serve as a significant source of trace gases, including NO_x, HONO, reactive halogens, and organic compounds.[15,16]

Despite the first direct observation of ambient HONO in urban Jülich, Germany, in spring 1979,[17] the atmospheric

Received: January 26, 2019
Revised: March 22, 2019
Accepted: March 26, 2019
Published: March 26, 2019

DOI: 10.1021/acsearthspacechem.9b00023
ACS Earth Space Chem. XXXX, XXX, XXX−XXX

HONO budget is still not well constrained, mainly due to the lack of measurements and limited knowledge about HONO production.[18] Sparse observations around the globe show that HONO mole fractions range from a few parts per trillion (ppt = pmol mol^{-1}) in clean environments[19−22] to a few parts per billion (ppb, nmol mol^{-1}) in polluted environments.[2,23] HONO can be emitted into the atmosphere directly through vehicle exhaust[24−27] and other combustion processes.[28−31] HONO sources also include gas-phase NO oxidation by OH (R1),[18] heterogeneous hydrolysis of nitrogen dioxide (NO_2) on aerosols (R2),[32] photosensitized reduction of NO_2 on humic acid aerosols,[33,34] reduction of NO_2 on soot,[35] and photolysis of particulate nitrate (R3).[36−38]

$$NO + OH + M \rightarrow HONO + M \quad (R1)$$

$$2NO_2 + H_2O_{(aq)} \rightarrow HONO + HNO_{3(aq)} \quad (R2)$$

$$NO^-_{3(aq)} + h\upsilon\ (\lambda > 290\ nm) + H^+ \rightarrow NO_{2(aq)} + OH_{(aq)} \quad (R3)$$

Vertical gradient measurements of HONO suggest that ground surfaces could be a large/dominant tropospheric HONO source.[19,20,39−43] These sources include heterogeneous hydrolysis of NO_2 and photolysis of HNO_3/nitrate on ground/snow surfaces,[19,43,44] biological processes in soil[45−47] and snow,[48] and acid displacement by atmospheric nitric acid (HNO_3) and hydrochloric acid (HCl).[49] HONO is removed from the troposphere mainly through photolysis (R4),[50] oxidation by OH (R5) and Cl radicals,[51] and deposition to the ground.[49,52]

$$HONO + h\upsilon\ (300\ nm < \lambda < 405\ nm) \rightarrow NO + OH \quad (R4)$$

$$HONO + OH \rightarrow NO_2 + H_2O \quad (R5)$$

In the atmosphere, HONO can dissolve and dissociate in cloud, fog, dew, and particulate water to form $HONO_{(aq)}$ and $NO^-_{2(aq)}$ (R6), with a Henry's law constant (H_{HONO}) of 48 M atm^{-1} and an acid dissociation constant (K_6) of 5.3×10^{-4} M at 25 °C.[53] In addition, the nitroacidium ion ($H_2ONO^+_{(aq)}$) can be formed in acidic solution (e.g., particles) (R7), with an equilibrium constant (K_7) of ≈0.02 M.[54,55] Particulate nitrite (pN(III); N(III) = $NO^-_{2(aq)}$ + $HONO_{(aq)}$ + $H_2ONO^+_{(aq)}$) undergoes thermodynamic partitioning processes with $HONO_{(g)}$.[56] However, particulate nitrite concentrations are seldom reported, with concentrations generally ranging from 0.005 to 2 μg m^{-3}.[23,56−65] The sources of particulate nitrite include particulate nitrate photolysis,[16,22,36,66] NO_2 hydrolysis,[32] and uptake of HONO by particles.[67,68] The sinks of particulate nitrite include photolysis,[69] particle-phase oxidation by O_3[70] and OH,[71] release into the atmosphere as $HONO_{(g)}$, and deposition.

$$HONO \leftrightarrow HONO_{(aq)} \leftrightarrow NO^-_{2(aq)} + H^+_{(aq)} \quad (R6)$$

$$HONO_{(aq)} + H^+_{(aq)} \leftrightarrow H_2ONO^+_{(aq)} \quad (R7)$$

While HONO likely partitions between the atmosphere and snow grains,[58,72] snow nitrite (sN(III)) concentrations have seldom been reported. Snow nitrite concentrations of 0.01−0.18 μM have been measured above the coastal tundra in Utqiaġvik, Alaska, during spring.[58,72] Zuo et al.[73] observed higher snow nitrite concentrations (0.46−0.70 μM) at suburban North Dartmouth, Massachusetts, during winter. In Ny-Ålesund, Svalbard, during spring, snow nitrite concentrations ranged from 1 to 10 μM for about half of the snow samples, with the other half at <1 μM; Amoroso et al.[48] proposed that the high snow nitrite levels were caused by microbial oxidation of ammonium from clay minerals based on the isotopic analysis of snow nitrite and nitrate. Snow nitrite can originate from snow nitrate photolysis in the snow quasi-liquid layer (R8),[16,20,74] NO_2 hydrolysis,[75] uptake of $HONO_{(g)}$,[72] microbial oxidation of NH^+_4,[48] and deposition of particulate nitrite onto the snowpack.[58] Snow nitrate from the deposition of $HNO_{3(g)}$ and particulate nitrate plays an important role in the near-surface NO_x and HONO budgets when nitrate photolysis releases NO_2 and HONO back into the atmosphere (R3 and R8).[16] Laboratory studies suggest that R3 proceeds about 10 times faster than R8 in both aqueous and ice phases.[76,77] Sinks of snow nitrite include photolysis[69] and oxidation by O_3[70] and OH[71] in the snow grains, leading to a release of HONO into the snow interstitial air and atmosphere.

$$NO^-_{3(aq)} + h\upsilon\ (\lambda > 290\ nm) \rightarrow NO^-_{2(aq)} + O(^3P)_{(aq)} \quad (R8)$$

Wintertime air pollution in the midwest United States is characterized by high fractions of particulate ammonium nitrate, often over snow-covered ground.[78] As a consequence, the photolysis of nitrate in aerosol particles and snowpack are expected to inject significant amounts of HONO and NO_2 into the near-surface atmosphere, thereby significantly influencing the oxidative capacity of the wintertime urban atmosphere. Here, we describe field observations in the snow-covered urban winter environment of Kalamazoo, Michigan. Assisted with meteorological data, we analyzed the temporal variability of ambient $HONO_{(g)}$, particulate nitrite and nitrate, and snow nitrite and nitrate to investigate the importance of the snowpack and atmospheric particles for $HONO_{(g)}$ production. We compared the calculated contributions of HONO photolysis and O_3 photolysis to OH production, at ≈2 m above ground, to investigate the role of HONO in the oxidative capacity of the near-surface atmosphere. To our knowledge, this is the first study to simultaneously measure ambient $HONO_{(g)}$, particulate nitrite and nitrate, and snow nitrite and nitrate at a midlatitude urban site.

EXPERIMENTAL SECTION

The Snow and Atmospheric Chemistry in Kalamazoo (SNACK) 2018 winter campaign was conducted in an open field (42.28°N, 85.61°W) adjacent (≈90 m) to a major road, on the campus of Western Michigan University (WMU) in Kalamazoo, Michigan, from January 12 to February 24, 2018. A nonorthogonal, three-dimensional sonic anemometer (model CSAT3, Campbell Scientific Inc., Logan, UT) was installed 1.4 m above the ground to measure the sonic air temperature (T_{air}) and three-dimensional wind speed (u = zonal wind speed, v = meridional wind speed, and w = vertical wind speed) at 20 Hz starting on January 20, 2018. Friction velocity ($u^* = \sqrt[4]{\overline{u'w'}^2 + \overline{v'w'}^2}$) was calculated from turbulent covariance of the 3-D wind speed based on 30 min averaging,[79] where u', v', and w' are fluctuations about the mean wind speed. For January 12−19 and February 20−21, air temperatures and wind speeds were obtained from the Kalamazoo−Battle Creek International Airport (KAZO) located about 7 km to the southeast (https://www.wunderground.com/history/daily/us/mi/kalamazoo/KAZO). The difference be-

DOI: 10.1021/acsearthspacechem.9b00023
ACS Earth Space Chem. XXXX, XXX, XXX−XXX

tween the temperature measured at the field site and at KAZO during the overlapping periods was generally within 1 °C. Relative humidity (RH) was obtained from the KAZO station. Water vapor concentrations ($[H_2O]$) were calculated from T_{air} and RH (E1).[80] Solar ultraviolet (UV) actinic flux (wavelength from 0.295 to 0.385 μm) above the ground was measured using an UV radiometer (Model TUVR, Eppley Laboratory Inc., Newport, RI) starting on January 28, 2018. We define two ground types, snow-covered ground and bare-soil ground, based on daily photos taken at the field site. The days with snow-covered ground were January 12−21, January 30, and February 2−19. The rest of the days during the campaign were with bare-soil ground.

$$[H_2O] = RH(a + b\Delta T_{air} + c(\Delta T_{air})^2 + d(\Delta T_{air})^3 + e(\Delta T_{air})^4 + f(\Delta T_{air})^5 + g(\Delta T_{air})^6) \quad \text{(E1)}$$

where a = 6.11, b = 4.44 ×10^{-1}, c = 1.43 ×10^{-2}, d = 2.65 ×10^{-4}, e = 3.03 ×10^{-6}, f = 2.03 ×10^{-8}, g = 6.14 ×10^{-11}, and $\Delta T_{air} = T_{air} - 273.15$.

Inorganic trace gases (HONO, NH_3, and SO_2 measured as NO_2^-, NH_4^+, and SO_4^{2-}, respectively) and particle-phase ions (NO_2^-, NO_3^-, SO_4^{2-}, Cl^-, NH_4^+, K^+, Mg^{2+}, and Ca^{2+}) were measured by an ambient ion monitor coupled to anion and cation ion chromatographs (AIM-IC; model 9000D, URG Corp., Chapel Hill, NC). Details about the AIM-IC instrument and its performance and accuracy in measuring HONO, particulate nitrite, and other inorganic trace gases and particle-phase ions in the lab and field are described by Markovic et al.[81,82] and VandenBoer et al.[56] Briefly, air was sampled at 3 L min^{-1} through a 2.5 μm cyclone, located at 1.8 m above ground, to remove coarse particles (>2.5 μm), and then immediately directed through a parallel-plate wet denuder, where soluble inorganic trace gases diffused through the PTFE Teflon membranes constantly supplied with H_2O_2 solution at 10 mL h^{-1}. Particles entered a supersaturation chamber where hygroscopic growth was initiated, followed by collection in an inertial particle separator. The parallel-plate wet denuder and supersaturation chamber were located outside in a heated (≈10 °C) aluminum case to prevent sampling line artifacts, freezing, and photolytic degradation of samples. The collected dissolved trace gases and particles were separately sent to two different ICs (ICS-1100 for cations and ICS-2100 for anions; Dionex Inc., Sunnyvale, CA) for measurements of both cation and anion concentrations. Lithium fluoride (LiF) was used as the internal standard. Samples were collected on concentrator columns (anion, UTAC-ULP1, ultra trace anion concentrator ultralow pressure; cation, TCC-ULP1, trace cation concentrator ultralow pressure; Thermo Fisher Scientific, Waltham, MA), with IC analyses every 2−4 h during the campaign to enable sufficient collection of low-abundance HONO and particulate nitrite from the ambient air (sampling time was set to 3 h after January 24). Due to the varying time resolution, HONO and particulate nitrite and nitrate concentration diurnal average plots shown in this work were constructed using the average concentration for each hour; for example, for the 3-h time resolution, the same concentration was used for each hour of that period, because the measurement value represents an average concentration for the 3 h period. The 3-h 3σ limits of detection (LODs) for HONO and particulate nitrite and nitrate were 1 ppt, 0.002 μg m^{-3}, and 0.05 μg m^{-3}, respectively. Ozone was measured at a flow rate of 1.7 L min^{-1} using an ozone monitor (Model 205, 2B Technologies Inc., Boulder, CO) coupled with an FEP tubing inlet (1/4″ OD); the O_3 LOD was 1 ppb.

Thirty-eight surface snow (top 2 cm) samples were collected at the field site between February 4 and February 18. After February 18, the snow melted completely. The surface snow samples were collected using a polypropylene scoop while wearing disposable polyethylene gloves. Twenty of the surface snow samples were collected around sunset (16:00−19:00 Eastern Standard Time (EST)), and the rest of the surface snow samples were collected before sunrise (21:00−07:00 EST). The snow density (ρ_{snow}) was measured in the field with a snow density gauge (Scientist 200, Brooks-Range Inc., Fremont, CA). Snow samples were stored in a −20 °C freezer at WMU, then transferred to a −30 °C freezer at the University of Michigan, and were melted as needed prior to IC analysis and pH measurement. Li[58] repeated anion measurements (NO_2^-, NO_3^-, SO_4^{2-}, Cl^-, and Br^-) of particle samples 2−8 months after the initial sample extraction to investigate the sample stability in the frozen aqueous filter extract solution and found no detectable deterioration over the 8 month period. Thus, we expect negligible deterioration of our snow samples before measuring their anion and cation concentrations 4−7 months after collection. The pH of each melted snow sample was measured using a pH meter (Fisher Scientific Accumet AP110). The 200 μL of each melted snow sample was loaded through a 0.2 μm filter using sterile single-use syringes (Luer-Lok 1-mL, Becton, Dickinson and Company, Franklin Lakes, NJ) into each IC for cation (Dionex ICS-1100; NH_4^+, Na^+, K^+, Mg^{2+}, and Ca^{2+}) and anion (Dionex ICS-2100; NO_2^-, NO_3^-, SO_4^{2-}, Cl^-, and Br^-) measurements, respectively. The LODs (3σ) for snow NO_2^- and snow NO_3^- analyses were 0.002 and 0.07 μM, respectively.

We investigated the thermodynamic partitioning between HONO and particulate nitrite using aerosol pH and liquid water content calculated from the Extended Aerosol Inorganics Model II (E-AIM;[83] http://www.aim.env.uea.ac.uk/aim/model2/model2b.php). Observations of T_{air}, RH, particulate nitrate, sulfate, and ammonium, and gas-phase ammonia were used as inputs to calculate aerosol pH and liquid water content, assuming no solid formation[84] across the full range of observed RH (39−100%; averaged 75 ± 13% (1σ)). It is reasonable to assume particles to be deliquesced at such relative humidities, especially because particles often experience multiple cycles of varying RH.[84]

The photolysis frequencies of HONO (j_{HONO}) and O_3 (j_{O_3}) were obtained from the Tropospheric Ultraviolet and Visible (TUV) Radiation Model version 5.3.1, which considers the climatological O_3 column (340 DU), aerosol optical depth (0.235), surface albedo (0.8 for snow-covered ground and 0.17 for bare-soil ground[85]), and solar zenith angle (https://www2.acom.ucar.edu/modeling/tropospheric-ultraviolet-and-visible-tuv-radiation-model). The Eppley UV actinic flux (0.295−0.385 μm) output from the TUV model was compared with observations from the UV radiometer to correct for the uncertainties in the model inputs and cloud cover by multiplying the modeled photolysis frequency by the ratio of (observed UV)/(modeled UV), following Zhou et al.[44] and Kleinman et al.[86]

RESULTS AND DISCUSSION

HONO Observations above Snow-Covered Ground Compared with Bare-Soil Ground. During January−

DOI: 10.1021/acsearthspacechem.9b00023
ACS Earth Space Chem. XXXX, XXX, XXX−XXX

February in Kalamazoo, Michigan, ambient HONO mole fractions varied from 10 to 341 ppt, with an average of 54 ± 41 ppt (1σ) (Figure 1). HONO was, on average, 44% higher

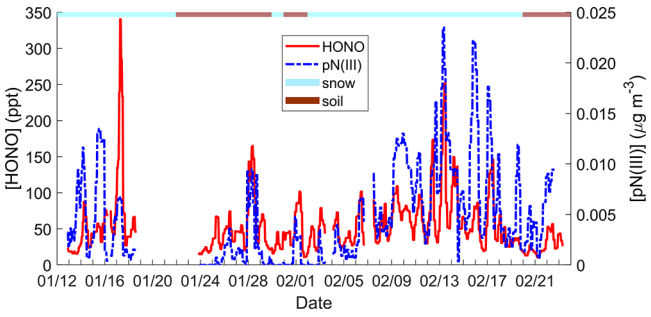

Figure 1. Time series of gas-phase HONO mole fractions ([HONO]) and particulate nitrite concentration ([pN(III)]) in Kalamazoo, Michigan. Ground types are shown as horizontal bars at top, snow (snow-covered ground) and soil (bare-soil ground).

above snow-covered ground (60 ± 44 ppt) than bare-soil ground (42 ± 30 ppt) (significant at 95% confidence level, $p = 7 \times 10^{-10}$). In comparison, during springtime NO_x pollution events in Utqiaġvik, Alaska, Villena et al.[87] found HONO mole fractions reached about 500 ppt above snow-covered ground. At a midlatitude suburban site near Paris, France, during winter, Michoud et al.[12] also observed high HONO mole fractions (500−4000 ppt) above snow-covered ground and proposed a snowpack HONO source, based on similar observed ambient NO_x concentrations and boundary layer heights above both snow-covered and snow-free ground.

The HONO diurnal patterns of above snow-covered ground and bare-soil ground are shown in Figure 2a. In general, HONO mole fractions over snow-covered ground were higher than over bare-soil ground throughout the day (on average, 87 versus 56 ppt at noon). Over snow-covered ground, HONO reached a peak of 87 ppt, on average, at noon, consistent with a light-dependent source. HONO mole fractions then decreased sharply after noon, reaching 34 ppt, on average, at 19:00 EST (just after sunset). Zhou et al.[19] also observed a noontime peak in HONO in the Arctic during spring and suggested snowpack nitrate photolysis resulting in HONO production. In comparison, Acker et al.[88] observed a noontime peak in HONO at a rural site in Germany during summer; this was suggested to be due to the photoenhanced uptake of NO_2 on organic films on ground and vegetation surfaces.[89]

The significant noontime peak in HONO was not observed over bare-soil ground (Figure 2a). The hourly average HONO was relatively stable between midnight and noon (fluctuating within the range of 50−56 ppt between 01:00 and 12:00 EST), and dropped from 56 to 23 ppt between 12:00 and 19:00 EST. The magnitude of decrease between 12:00 and 19:00 was much larger over snow-covered ground (from 87 to 34 ppt, on average). The absence of a noontime HONO peak over bare-soil ground suggests photoenhanced uptake of NO_2 on the ground[88] is not a dominant source of HONO in Kalamazoo during winter, and that some contributing HONO sources are likely not light-dependent, for example, NO_2 hydrolysis. This further suggests that snowpack nitrate photolysis, rather than photoenhanced uptake of NO_2 on the snowpack, is more likely the cause of the noontime HONO peak over snow-covered ground. As discussed in the Snow Nitrite as a Source of HONO section, a positive correlation between surface

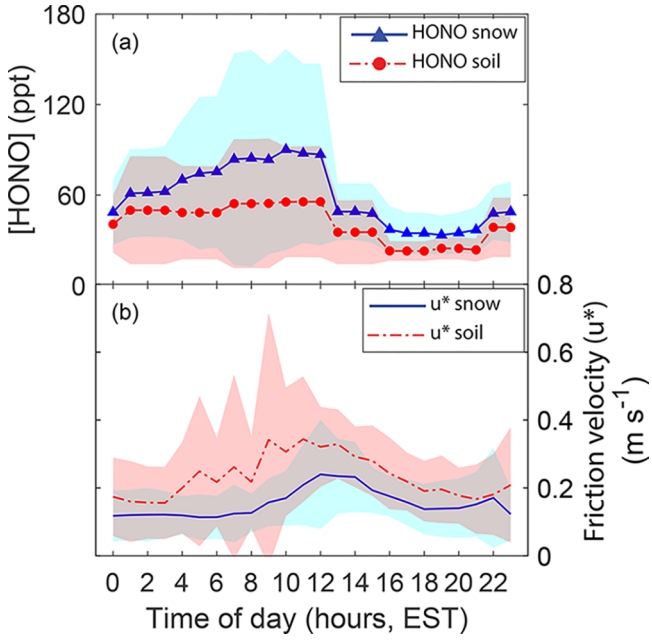

Figure 2. Diurnal patterns of average (a) HONO mole fractions ([HONO]) and friction velocities (u^*) for periods characterized by snow-covered (blue) and bare-soil ground (red). Since the AIM-IC sampling time was varied from 2 to 4 h during this campaign, the diurnal average plots shown were constructed using the average concentration for each hour, as described in the Experimental Section. The standard deviations of [HONO] and friction velocity are shown as shading.

snowpack nitrite and nitrate concentrations was observed (Figure 4), supporting nitrite production from nitrate photolysis, followed by HONO emission from the snowpack.

Turbulent mixing in the atmospheric boundary layer likely affected the observed diel patterns in HONO. The strength of turbulent mixing can be assessed by the friction velocity (u^*).[90] Figure 2b shows the diurnal pattern of u^* over both snow-covered and bare-soil ground. Overall, the friction velocity was lower over snow-covered ground than bare-soil ground (on average, 0.16 ± 0.10 versus 0.23 ± 0.16 m s^{-1}), indicating weaker turbulent mixing over snow-covered ground. Over snow-covered ground, friction velocity peaked around noon, coinciding with the HONO noontime peak. The reduced vertical mixing in the morning, compared to noon, likely contributed to the elevated morning HONO mole fractions (Figure 2a) by trapping surface-produced HONO near the ground. Stronger turbulent mixing at noon promoted vertical transport of HONO emitted from the snowpack, thereby countering increased HONO production and resulting in the diel pattern of HONO not following that of actinic flux.

Particulate Nitrite not in Thermodynamic Equilibrium with HONO. NO_2 hydrolysis and nitrate photolysis in atmospheric particles produce HONO (R2, R3, and R8).[32,36] Particles also provide surfaces for HONO uptake.[56] In Kalamazoo, the particulate nitrite concentrations ([pN(III)]) varied from below LOD (0.002 μg m^{-3}) to 0.024 μg m^{-3} (Figure 1), with an average of 0.005 ± 0.005 μg m^{-3} (1σ). This is similar to the average particulate nitrite concentration of 0.005 μg m^{-3} at an Arctic site (Utqiaġvik, Alaska) during spring 1986−1989,[58] but much lower than at larger midlatitude cities during winter (0.2 μg m^{-3} in Salt Lake City, Utah;[64] 0.4 μg m^{-3} in Beijing, China;[62] and 2.1 μg m^{-3} in

DOI: 10.1021/acsearthspacechem.9b00023
ACS Earth Space Chem. XXXX, XXX, XXX−XXX

Ji'nan, China[23]). On average, particulate nitrite concentrations during periods with snow-covered ground (0.006 ± 0.005 μg m^{-3}) were about twice as high as for bare-soil ground periods (0.003 ± 0.003 μg m^{-3}) (Figure 3a). In general, the diurnal

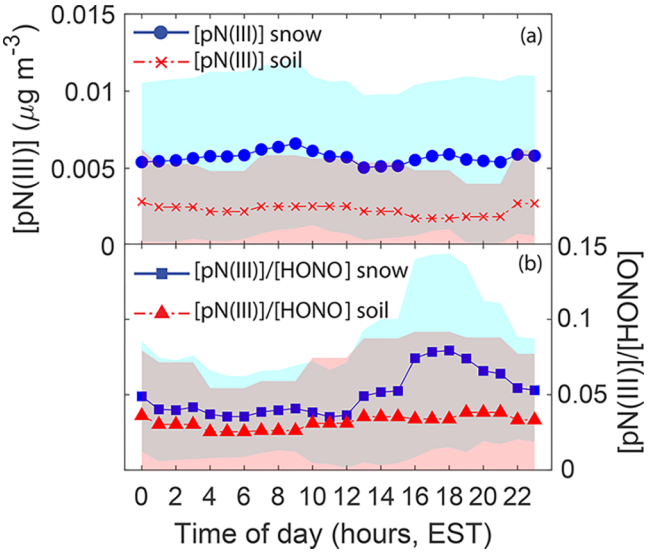

Figure 3. Diurnal patterns of average (a) particulate nitrite concentrations ([pN(III)]) and (b) [pN(III)]/[HONO] ratios above snow-covered and bare-soil ground. The standard deviations of [pN(III)] and [pN(III)]/[HONO] are shown as shading.

variations in particulate nitrite over both snow-covered and bare-soil ground were smaller than for HONO. In contrast to HONO, a noontime peak of particulate nitrite was neither observed on snow-covered ground nor bare-soil ground. Over snow-covered ground, hourly average particulate nitrite concentrations fluctuated between 0.005 and 0.007 μg m^{-3} throughout the day (Figure 3a). In comparison, over bare-soil ground, hourly average particulate nitrite concentrations were lower, at ~0.002−0.003 μg m^{-3}.

The average particulate nitrite to HONO concentration ratio ([pN(III)]/[HONO]) during this winter study was 0.04 ± 0.04 (1σ), which is smaller than the few values reported in previous literature (average of 0.25 in Bakersfield, California, during May−July;[56] range of 0.29−0.69 in Zurich, Switzerland, during August−September;[63] average of 1.6 in Lubbock, Texas, in November;[59] average of 1.86 in Seoul, Korea, during May−July;[65] and average of 4.26 in Beijing, China, during November−January[23]). Particulate nitrite undergoes thermodynamic exchange processes with HONO in the atmosphere.[56] The E-AIM model was used to predict particle pH and liquid water content (Experimental Section) to enable the calculation of the thermodynamic equilibrium between particulate nitrite and HONO ([pN(III)]/[HONO] ratio) (R6 and R7). On average, the particle pH and liquid water content predicted from E-AIM were 3.2 and 3.5 × 10^{-9} g m^{-3}, respectively, for an average T_{air} of −1.7 °C and RH of 75%. Using the particle pH and liquid water content (LWC) predicted from E-AIM, the [pN(III)]/[HONO] ratio was calculated (E2)[91] to be 6 × 10^{-8}, which is much smaller than our observations (0.05 ± 0.04 over snow-covered ground and 0.03 ± 0.04 over bare-soil ground). This suggests particulate nitrite was supersaturated, with particles likely representing a source of HONO.[23,57]

$$\frac{[\mathrm{pN(III)}]}{[\mathrm{HONO}]} = H_{\mathrm{HONO}}\left(1 + \frac{K_6}{[\mathrm{H^+}]} + \frac{[\mathrm{H^+}]}{K_7}\right)RT_{\mathrm{air}}\mathrm{LWC} \quad \text{(E2)}$$

R is the gas constant. The LWC is the particle liquid water content. The [H$^+$] is the hydrogen ion concentration, obtained from the predicted particle pH.

The supersaturation of particulate nitrite in our observations compared to the thermodynamic equilibrium approximation could be due to several reasons. The aerosol pH and liquid water content calculated from the E-AIM model could be incorrect. However, in order to reproduce the [pN(III)]/[HONO] observations, aerosol liquid water content would need to increase by 6 orders of magnitude, which is unrealistic. Alternately, aerosol pH would need to increase by 6 units, which is unlikely, except for alkaline particles. Particulate nitrite may reside predominantly on lofted alkaline dust or road salt particles. VandenBoer et al.[49,56] suggested high [pN(III)]/[HONO] ratios could be caused by the uptake of HONO onto soil and/or lofted alkaline agricultural soil particles. Solid formation of nitrite could have occurred in the particles, since the E-AIM model does not include either aqueous-phase or solid-phase nitrite (e.g., NH_4NO_2 and $NaNO_2$). In our study, high observed [pN(III)]/[HONO] ratios (compared to calculated) occurred both above snow-covered ground and bare-soil ground (Figure 3b), suggesting that the uptake of HONO onto soil/dust alone cannot explain the ratios. Since road salt is omnipresent in the wintertime,[92] it is likely that road salt particles took up HONO, but the mixing state of nitrite is not known for wintertime in Kalamazoo to confirm this assumption. The increase in the observed [pN(III)]/[HONO] ratio in the late afternoon over snow-covered ground (Figure 3b) was caused by the decrease in HONO abundance at that time, indicating that the [pN(III)]/[HONO] diurnal pattern over snow-covered ground was driven by the HONO diurnal pattern that was affected by snow nitrate photolysis.

Snow Nitrite as a Source of HONO. The nitrite concentration in the Kalamazoo surface (top 2 cm) snow samples varied from 0.04 to 1.99 μM, with an average of 0.4 ± 0.3 μM (1σ), which is similar to previous snow nitrite measurements (0.46−0.70 μM) in southeast Massachusetts during winter.[73] The observed levels are higher than the 0.01−0.18 μM of snow nitrite measured at Utqiaġvik, Alaska, during spring,[58,72] as expected due to the higher anthropogenic NO_x emissions at the midlatitude urban sites. The average nitrite concentration for snow samples collected around sunset was 0.5 ± 0.4 μM, while the average nitrite concentration for snow samples collected at night was 0.3 ± 0.1 μM, but the difference is not significant at the 95% confidence level.

Here we investigate whether snow nitrite concentrations measured in this study were high enough for the ground snowpack to potentially be a significant source of HONO to the ambient air. HONO in contact with the snowpack undergoes adsorption equilibrium with nitrite at the snowpack surface,[72,93−95] as parametrized in E3 and E4

$$[\mathrm{HONO_{(g,eq)}}] = \frac{[\mathrm{HONO_{(sn,surf)}}]}{K_{\mathrm{linC}}} \quad \text{(E3)}$$

$$[\mathrm{HONO_{(sn,surf)}}] = \frac{[\mathrm{HONO_{(sn,bulk)}}]N_A\rho_{\mathrm{ice}}}{10^3 A_{\mathrm{sn}}} \quad \text{(E4)}$$

DOI: 10.1021/acsearthspacechem.9b00023
ACS Earth Space Chem. XXXX, XXX, XXX−XXX

where $[HONO_{(g,eq)}]$ (molecule m^{-3}) is the HONO gas concentration close to the snowpack surface; $[HONO_{(sn,surf)}]$ (molecule m^{-2}) is the snowpack surface nitrite number density; the gas-ice partition coefficient for HONO $K_{linC} = 1.5 \times 10^{-10}\exp(5200/T_{snow})$ m;[95] the Avogadro's number $N_A = 6.02 \times 10^{23}$ molecule mol^{-1}; $\rho_{ice} = 917$ kg m^{-3} is the ice density; and A_{sn} (m^2 kg^{-1}) is the snow specific surface area, which could vary from 2 m^2 kg^{-1} for melt-freeze crusts, 20 m^2 kg^{-1} for aged snow, to 160 m^2 kg^{-1} for fresh snow in the Arctic and French Alps snow samples.[96,97] Using the average measured snow temperature (T_{snow}) of 268 K, $[HONO_{(sn,bulk)}]$ of 0.4 μM, and A_{sn} of 20−160 m^2 kg^{-1}, we calculate $[HONO_{(g,eq)}]$ to be 3−28 $\times 10^{16}$ molecule m^{-3}, which is 1−10 ppb. In comparison, the average HONO mole fraction measured at 1.8 m above the ground in this study was only 54 ppt, which is much smaller than the calculated $[HONO_{(g,eq)}]$, suggesting a large HONO emission from the snowpack to the ambient air. Using the same adsorption equilibrium method (E3 and E4), Jacobi et al.[72] suggested that the snowpack could act as a source during low (<15 ppt) HONO abundance periods and a sink during high (100−500 ppt) HONO abundance periods. In our study, the calculated $HONO_{(g,eq)}$ levels close to the snowpack surface were always higher than the measured HONO levels at 1.8 m, supporting the hypothesis that the snowpack primarily serves as a HONO source.

A positive correlation was found between snow nitrite and nitrate concentrations (R^2 = 0.7) (Figure 4), suggesting

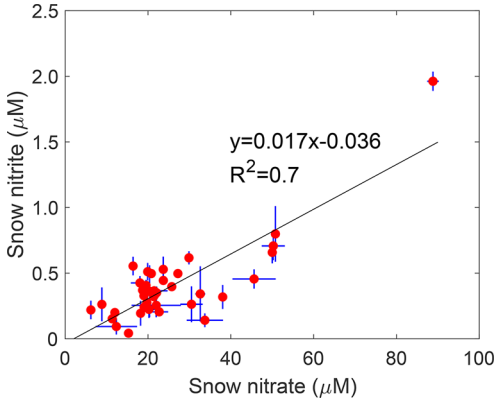

Figure 4. Snow nitrite concentration versus snow nitrate concentration for all surface snow samples.

production of snow nitrite from snow nitrate photolysis.[19] The snow nitrite/nitrate ratio varied from 0.003 to 0.035 for all surface snow samples, with an average of 0.016 ± 0.007 (1σ). In comparison, the average snow nitrite/nitrate ratio was measured to be 0.08 in suburban north Dartmouth, Massachusetts, during winter[73] and 0.007 in Utqiaġvik, Alaska, during spring.[72] Note, that the snow nitrite and nitrate measurements shown above are all bulk concentrations in the snowpack. One needs to know the physical and chemical properties of the disordered interface to estimate snow nitrite and nitrate concentrations in that layer,[91,98] because liquid channels exist in the entire ice and some fraction of the ice surface consists of bare ice.[99] Only snow nitrite in liquid regions at the air interface is expected to exchange with HONO close to the snow surface, limiting the potential HONO production, compared to the bulk nitrate present.

OH Production from HONO and O_3 Photolysis. HONO affects the oxidative capacity of the atmosphere via photolysis to produce OH (R3). Regardless of its low abundance, HONO could represent a larger source of OH in the atmosphere than O_3, as the photolysis frequency of HONO (j_{HONO}) is about 2 orders of magnitude higher than that of O_3 ($j_{O(^1D)}$).[1,100] This is especially evident at the wintertime midwest US, where water vapor abundance ($[H_2O]$) is low (on average 1.2×10^{17} molecules cm^{-3}, calculated from T_{air} and RH in this study) mainly due to the low T_{air} (on average −3 °C) during this study. The OH production mechanism from O_3 photolysis is shown in R9−R12.[101] O_3 photolysis produces $O(^1D)$, followed by the reaction with water vapor to form OH.

$$O_3 + h\upsilon\ (\lambda \le 330\ nm) \rightarrow O(^1D) + O_2 \quad (R9)$$

$$O(^1D) + H_2O \rightarrow 2OH \quad (R10)$$

$$O(^1D) + N_2 \rightarrow O(^1P) + N_2 \quad (R11)$$

$$O(^1D) + O_2 \rightarrow O(^1P) + O_2 \quad (R12)$$

Figure 5 shows the diurnal patterns of the calculated OH production rates, in the near-surface atmosphere at ≈2 m

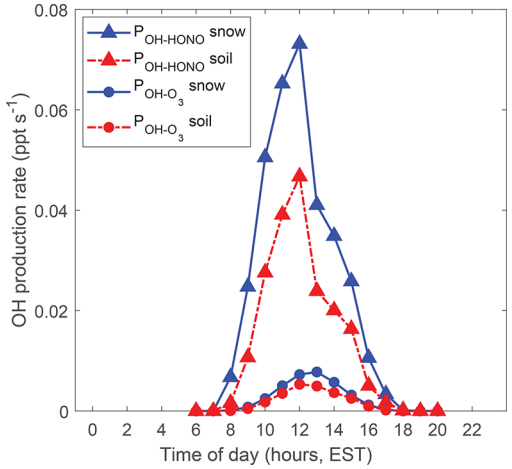

Figure 5. Diurnal patterns of average calculated OH production rates from measured HONO ($P_{OH-HONO}$) and O_3 (P_{OH-O_3}) above snow-covered and bare-soil ground.

above ground, from photolysis of measured HONO ($P_{OH-HONO}$) and O_3 (P_{OH-O_3}) in Kalamazoo. $P_{OH-HONO}$ and P_{OH-O_3} were calculated from E5 and E6, respectively.

$$P_{OH-HONO} = j_{HONO}[HONO_{(g)}] \quad (E5)$$

$$P_{OH-O_3} = \frac{2j_{O(^1D)}k_{10}[H_2O][O_3]}{k_{10}[H_2O] + k_{11}[N_2] + k_{12}[O_2]} \quad (E6)$$

k_{10} (=$2.0 \times 10^{-10}\exp(60/T_{air})$ cm^{-3} $molecule^{-1}$ s^{-1}), k_{11} (=$3.1 \times 10^{-11}\exp(110/T_{air})$ cm^{-3} $molecule^{-1}$ s^{-1}), and k_{12} (=$4.0 \times 10^{-11}\exp(55/T_{air})$ cm^{-3} $molecule^{-1}$ s^{-1}) are the rate constants of R10, R11, and R12, respectively.[50] The diurnal patterns of the average j_{HONO}, $j_{O(^1D)}$, $[O_3]$, T_{air}, and RH are shown in Figure 6. Calculated $P_{OH-HONO}$ and P_{OH-O_3} were both higher over snow-covered ground than over bare-soil ground, due to the higher abundances and photolysis frequencies of HONO and O_3 over snow-covered ground (Figures 2 and 5). In particular,

DOI: 10.1021/acsearthspacechem.9b00023
ACS Earth Space Chem. XXXX, XXX, XXX−XXX

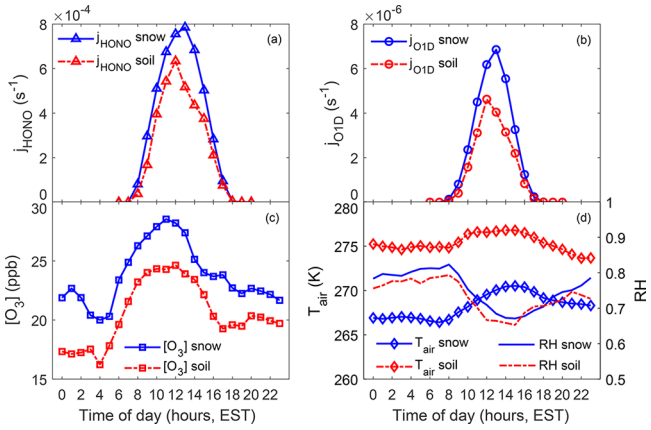

Figure 6. Diurnal patterns of the average calculated photolysis frequencies of (a) HONO (j_{HONO}) and (b) O_3 (j_{O^1D}), (c) measured O_3 mole fractions ($[O_3]$), (d) air temperature (T_{air}), and RH for time periods with snow-covered ground, compared to bare-soil ground.

$P_{OH\text{-}HONO}$ was on average 46% higher over snow-covered ground than bare-soil ground at noon. This indicates that the HONO production rate was 46% higher over snow-covered ground than bare-soil ground at noon under the photochemical steady state assumption (HONO lifetime of 10−30 min at noon during the SNACK campaign). However, this does not mean that the difference corresponds to snow nitrate photolysis only, since NO_x abundance may be different over snow-covered and bare-soil ground periods, especially due to the photochemical production of NO_x from the snowpack[16,111,112] and possible subsequent snow-phase hydrolysis of NO_2,[16,19,113] for example. Compared to P_{OH-O_3}, $P_{OH-HONO}$ was on average 10 times higher over snow-covered ground and on average seven times higher over bare-soil ground, suggesting the important role of HONO for OH production and the oxidative capacity of the near-surface atmosphere in the wintertime midlatitude urban environment, especially when snow is present. It should be noted, that both $P_{OH-HONO}$ and P_{OH-O_3} were calculated at the sampling height of ≈2 m above the ground, which does not represent OH production from HONO and O_3 throughout the entire boundary layer.[105,106] These results motivate future studies of vertically resolved HONO. Previous studies have found HONO to be more important than O_3 for OH production in cities, especially during winter.[2,9,102,103] In particular, in the highly polluted urban wintertime environment of Santiago, Chile (daytime average [HONO] ≈ 4 ppb and $[O_3]$ ≈ 20 ppb), Elshorbany et al.[2] calculated $P_{OH-HONO}$ to be more than 2 orders of magnitude higher than P_{OH-O_3}.

Contribution of Particulate Nitrate Photolysis to HONO Production. Here, we investigate the importance of particulate nitrate photolysis to HONO production during the SNACK campaign. Recent studies have suggested that sea spray aerosol nitrate photolysis represents a large source of HONO in the marine boundary layer.[22,36,38] In addition, for an aircraft field campaign over southeastern US during summer 2013, Ye et al.[37] suggested that particulate nitrate photolysis was the dominant (≈70%) source of HONO. Following the laboratory study of Ye et al.[36] and modeling studies of Reed et al.[104] and Kasibhatla et al.,[38] we assumed particulate nitrate photolysis produces 67% HONO and 33% NO_2, and the photolysis frequency of particle nitrate (j_{pNIT}) is 100 times the photolysis frequency of gas-phase HNO_3 (j_{HNO_3}). The j_{HNO_3} was obtained from the TUV model. Figure 7 shows the diurnal

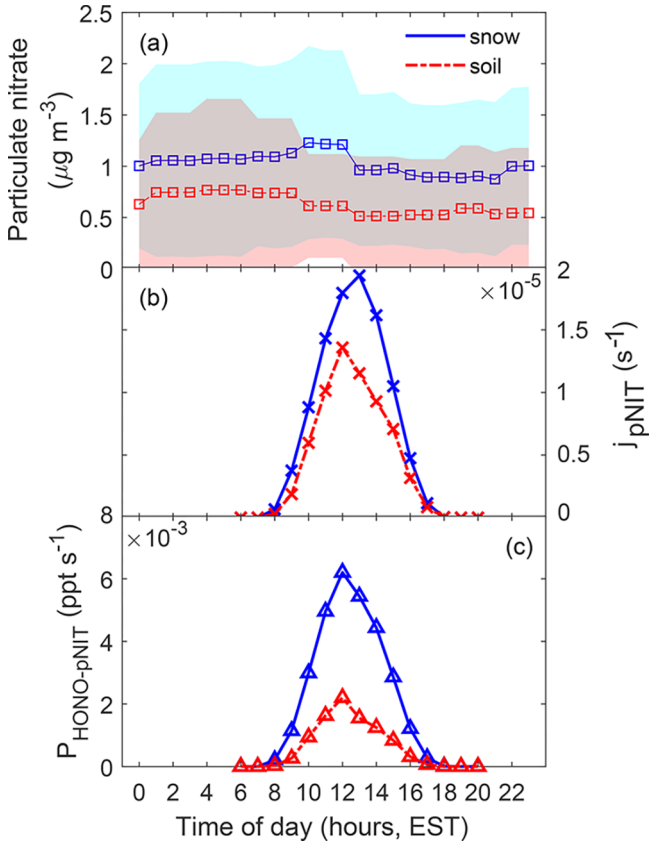

Figure 7. Diurnal patterns of (a) measured particulate nitrate concentrations, (b) calculated particulate nitrate photolysis frequencies (j_{pNIT}), and (c) calculated HONO production rate from particulate nitrate photolysis ($P_{HONO-pNIT}$) over snow-covered and bare-soil ground. The standard deviations of particulate nitrate concentrations are shown as shading in (a). Here we have assumed particulate nitrate photolysis produces 67% HONO and 33% NO_2, and particle nitrate photolysis frequency is 100 times greater than the gas-phase HNO_3 photolysis frequency.[36,38]

pattern of the average calculated HONO production rate from particulate nitrate photolysis ($P_{HONO\text{-}pNIT}$); the HONO production rate reached 0.006 and 0.002 ppt s^{-1}, on average, at noon over snow-covered ground and bare-soil ground, respectively. Since photolysis is the dominant HONO loss process,[18] the HONO production rate at noon can be approximated as the HONO photolysis rate ($P_{OH-HONO}$) under the photochemical steady state assumption, as discussed in the OH Production from HONO and O_3 Photolysis section. In comparison, $P_{OH-HONO}$ was 0.07 and 0.05 ppt s^{-1} at noon, on average, over snow-covered ground and bare-soil ground, respectively (Figure 5). Therefore, on average, $P_{HONO-pNIT}$ was only 8% of $P_{OH-HONO}$ over snow-covered ground and 5% over bare-soil ground at noon. Figure 8 shows the linear correlations between $P_{HONO-pNIT}$ and $P_{OH-HONO}$ over snow-covered ground and bare-soil ground, respectively. The slopes of 0.077 over snow-covered ground and 0.047 over bare-soil ground indicate particulate nitrate photolysis accounts for 7.7% and 4.7% of HONO production, respectively.[37] This suggests that particulate nitrate photolysis was only a minor source of HONO during the SNACK campaign, further supporting the

DOI: 10.1021/acsearthspacechem.9b00023
ACS Earth Space Chem. XXXX, XXX, XXX−XXX

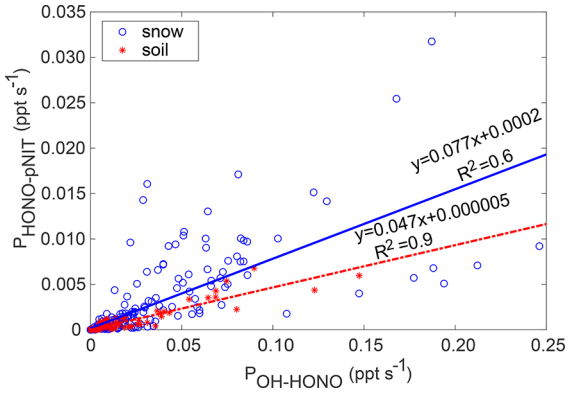

Figure 8. Correlation analysis of HONO production via particulate nitrate photolysis ($P_{HONO-pNIT}$) with HONO removal via photolysis ($P_{OH-HONO}$) over snow-covered ground (slope, 0.077; intercept, 0.0002; R^2 = 0.6) and bare-soil ground (slope, 0.047; intercept, 0.000005; R^2 = 0.9), respectively. As in Figure 7, we have assumed particulate nitrate photolysis produces 67% HONO and 33% NO_2, and particle nitrate photolysis frequency is 100 times greater than the gas-phase HNO_3 photolysis frequency.[36,38]

hypothesis that snowpack is a significant HONO source. Other HONO sources, such as NO_2 hydrolysis on particles[32] and snowpack[16,19,89] and NO oxidation by OH,[18] are likely important for HONO production; however, the importance of these sources unfortunately could not be evaluated due to lack of NO_x measurements. It should be noted, that j_{pNIT} is very uncertain, ranging from 1 to 100 times j_{HNO_3},[36,38,104,108] and the yield of HONO from particle nitrate photolysis could range from 67 to 93%.[38] By considering these uncertainties, $P_{HONO-pNIT}$ ranges from 0.00006 to 0.009 ppt s^{-1} at noon, on average. This suggests that particle nitrate photolysis is likely negligible for HONO production in this study.

Contribution of Snow Nitrate Photolysis to HONO Production. Following Zatko et al.,[107] the HONO production flux ($F_{HONO-sNIT}$; molecules cm^{-2} s^{-1}) from snow nitrate photolysis can be estimated as

$$F_{HONO-sNIT} = \int_0^{3z_e} j_0 e^{-z/z_e} [NO_3^-]_s Y_{HONO} \frac{\rho_{snow}}{\rho_{ice}} dz \quad \text{(E7)}$$

where z_e (cm) is the e-folding depth of UV actinic flux in the snowpack; j_0 is the nitrate photolysis frequency at the snowpack surface; $[NO_3^-]_s$ is the average measured bulk snow nitrate concentration (26 μM); Y_{HONO} is the HONO yield from snow nitrate photolysis; ρ_{snow} is the average surface snow density measured (230 kg m^{-3}); and ρ_{ice} = 0.917 kg l^{-1} is the ice density. Assuming a z_e of 2 cm,[107] snow nitrate concentration invariant through the photic zone (≈6 cm), j_0 of 1−100 times j_{HNO_3} (modeled and scaled by radiation),[36,38,104,108] and Y_{HONO} of 67−93%,[36,38] we calculate $F_{HONO-sNIT}$ to be 1−138 × 10^9 molecules cm^{-2} s^{-1} at noon. Previous studies have calculated HONO emission fluxes from the snowpack to range from 0.2 to 31 × 10^9 molecules cm^{-2} s^{-1} in different environments.[11,12,19,20,109] Notably, in the polluted Uintah Basin during wintertime, Zatko et al.[107] calculated fluxes of 0.2−3 × 10^9 molecules cm^{-2} s^{-1} at noon using a radiative transfer model and a snow chemistry model to calculate the HONO production rate from snow nitrate photolysis, for average snow nitrate concentrations of ≈100 μM.[107] It should be noted, that our estimate here is uncertain due to many assumptions, including scaling snow nitrate photolysis frequency to HNO_3 photolysis frequency, using a range of scaling factors based on laboratory experiments and estimates from field observations.[22,36−38,108] However, our estimated HONO snowpack emission flux is in line with previous measurement-derived fluxes in other environments, giving support to the estimated range here.

The effective HONO production rate in the near-surface atmosphere from snow nitrate photolysis ($P_{HONO-sNIT}$; ppt s^{-1}) is estimated as

$$P_{HONO-sNIT} = \frac{F_{HONO-sNIT}}{H_m \rho_{air}} \quad \text{(E8)}$$

where H_m (m) is the HONO effective mixing height, and ρ_{air}= 2.7 × 10^{19} molecules cm^{-3} (at an average measured T_{air} of −1.7 °C and pressure of 1 atm) is the air density. H_m can be estimated from eddy diffusivity (K_c; $m^2 s^{-1}$) derived from sonic anemometer measurements and HONO photolysis frequency (j_{HONO}; s^{-1}; modeled and scaled by radiation) as[110]

$$H_m = \sqrt{\frac{K_c}{j_{HONO}}} \quad \text{(E9)}$$

The average H_m was 20 m over snow-covered ground at noon in this study. With an $F_{HONO-sNIT}$ of 1−138 × 10^9 molecules cm^{-2} s^{-1}, $P_{HONO-sNIT}$ is calculated to be 0.02−2.56 ppt s^{-1} at noon. In comparison, the HONO production rate from particle nitrate photolysis is only 0.00006−0.009 ppt s^{-1} at noon (Contribution of Particulate Nitrate Photolysis to HONO Production section). Thus, particle nitrate photolysis is negligible compared to snow nitrate photolysis for HONO production within the HONO effective mixing height of 20 m. In comparison to the OH production rate from HONO over snow-covered ground (0.07 ppt s^{-1} at noon, on average), $P_{HONO-sNIT}$ (0.02−2.56 ppt s^{-1} at noon, on average) is estimated to account for 30−100% of total HONO production rate during daytime. It should be noted, that the calculated HONO production rate from snow nitrate photolysis ($P_{HONO-sNIT}$) is higher than the total HONO production rate ($P_{OH-HONO}$), when assuming j_0 is more than four times j_{HNO_3}. This suggests snow/particle nitrate photolysis may not be much faster than gas-phase HNO_3 photolysis, which is consistent with Romer et al.[108] (j_{pNIT} = 1−30 j_{HNO_3}). These calculations demonstrate the important role of snow nitrate photolysis in HONO production in the wintertime midlatitude urban environment.

CONCLUSIONS

In this study, the abundance of HONO and its contribution to the oxidative capacity of the atmosphere in the wintertime midlatitude snowy urban environment were investigated through measurements in January−February 2018 in Kalamazoo, Michigan. HONO mole fractions were, on average, 44% higher over snow-covered ground. The noontime peak in HONO over snow-covered ground suggests significant photochemical snowpack HONO emissions, likely from snow nitrate photolysis, as previously observed in the Arctic.[19] This is further supported by high snow nitrite concentrations (0.4 ± 0.3 μM) and the positive correlation between snow nitrite and nitrate concentrations. Particulate nitrate photolysis was found to be only a minor (<10%) source of HONO. Due to the high HONO abundance over snow-covered ground, the calculated OH production rate from HONO photolysis was, on average,

DOI: 10.1021/acsearthspacechem.9b00023
ACS Earth Space Chem. XXXX, XXX, XXX−XXX

an order of magnitude higher than that from O_3 photolysis on snow-covered ground, for the near-surface atmosphere (≈2 m above ground). The production of OH from HONO is especially important for the oxidative capacity of the atmosphere in the wintertime urban environment, where OH production via O_3 photolysis is limited due to low water vapor abundance.[9,10] It is important to note, that other species (e.g., HCHO photolysis and alkene ozonolysis) that were not measured in this campaign could also be important for OH production.[4] The snow-covered ground creates a stable and shallow boundary layer, reducing vertical mixing of trace gases and aerosols, and provides a high surface albedo to promote photochemical reactions.[13] In addition, the snowpack can serve as an important reservoir to recycle nitrogen species (e.g., nitrate, HONO, and NO_x) back into the atmosphere, which increases the lifetime of nitrogen species in the atmosphere.[16] Given elevated levels of particulate ammonium nitrate in the midwest US wintertime over snow-covered ground,[78] it is important to investigate the role of deposited nitrate on the midlatitude snowpack in the production of HONO.

AUTHOR INFORMATION

Corresponding Author

*E-mail: prattka@umich.edu.

ORCID

Kerri A. Pratt: 0000-0003-4707-2290

Notes

The authors declare no competing financial interest.

ACKNOWLEDGMENTS

This study was supported by the US National Science Foundation Atmospheric Chemistry program (award number 1738588), an Alfred P. Sloan Foundation Research Fellowship in Chemistry, and the University of Michigan. J.E. acknowledges funding from the Swiss National Science Foundation grant (155999). J.D.F. acknowledges support from the US National Science Foundation (award number 1417914). We thank Andrew Ault, Nicholas Ellsworth, and Matthew McNamara for assistance with preparing the mobile laboratory. We thank Peter Peterson, Guy Burke, and Alexa Watson (University of Michigan) for field logistical support. We thank Western Michigan University for use of their facilities for this study. We thank Jennifer Murphy and Milos Markovic (University of Toronto) for guidance modifying and deploying the AIM-IC.

REFERENCES

(1) Alicke, B.; Geyer, A.; Hofzumahaus, A.; Holland, F.; Konrad, S.; Patz, H. W.; Schafer, J.; Stutz, J.; Volz-Thomas, A.; Platt, U. OH formation by HONO photolysis during the BERLIOZ experiment. *J. Geophys. Res.-Atmos.* **2003**, *108* (D4), 1−17.

(2) Elshorbany, Y. F.; Kleffmann, J.; Kurtenbach, R.; Lissi, E.; Rubio, M.; Villena, G.; Gramsch, E.; Rickard, A. R.; Pilling, M. J.; Wiesen, P. Seasonal dependence of the oxidation capacity of the city of Santiago de Chile. *Atmos. Environ.* **2010**, *44*, 5383−5394.

(3) Elshorbany, Y. F.; Barnes, I.; Becker, K. H.; Kleffmann, J.; Wiesen, P. Sources and cycling of tropospheric hydroxyl radicals − an overview. *Z. Phys. Chem.* **2010**, *224*, 967−987.

(4) Stone, D.; Whalley, L. K.; Heard, D. E. Tropospheric OH and HO2 radicals: field measurements and model comparisons. *Chem. Soc. Rev.* **2012**, *41*, 6348−6404.

(5) Elshorbany, Y. F.; Steil, B.; Brühl, C.; Lelieveld, J. Impact of HONO on global atmospheric chemistry calculated with an empirical parameterization in the EMAC model. *Atmos. Chem. Phys.* **2012**, *12*, 9977−10000.

(6) Czader, B. H.; Rappenglück, B.; Percell, P.; Byun, D. W.; Ngan, F.; Kim, S. Modeling nitrous acid and its impact on ozone and hydroxyl radical during the Texas Air Quality Study 2006. *Atmos. Chem. Phys.* **2012**, *12*, 6939−6951.

(7) Elshorbany, Y. F.; Crutzen, P. J.; Steil, B.; Pozzer, A.; Tost, H.; Lelieveld, J. Global and regional impacts of HONO on the chemical composition of clouds and aerosols. *Atmos. Chem. Phys.* **2014**, *14*, 1167−1184.

(8) Li, Y.; An, J.; Kajino, M.; Gultepe, I.; Chen, Y.; Song, T.; Xin, J. Impacts of additional HONO sources on O3 and PM2.5 chemical coupling and control strategies in the Beijing−Tianjin−Hebei region of China. *Tellus, Ser. B* **2015**, *67* (1), 23930.

(9) Aumont, B.; Chervier, F.; Laval, S. Contribution of HONO sources to the NOx/HOx/O3 chemistry in the polluted boundary layer. *Atmos. Environ.* **2003**, *37*, 487−498.

(10) Kim, S.; VandenBoer, T. C.; Young, C. J.; Riedel, T. P.; Thornton, J. A.; Swarthout, B.; Sive, B.; Lerner, B.; Gilman, J. B.; Warneke, C.; Roberts, J. M.; Guenther, A.; Wagner, N. L.; Dube, W. P.; Williams, E.; Brown, S. S. The primary and recycling sources of OH during the NACHTT-2011 campaign: HONO as an important OH primary source in the wintertime. *J. Geophys. Res.-Atmos.* **2014**, *119*, 6886−6896.

(11) Beine, H.; Colussi, A. J.; Amoroso, A.; Esposito, G.; Montagnoli, M.; Hoffmann, M. R. HONO emissions from snow surfaces. *Environ. Res. Lett.* **2008**, *3*, No. 045005.

(12) Michoud, V.; Doussin, J.-F.; Colomb, A.; Afif, C.; Borbon, A.; Camredon, M.; Aumont, B.; Legrand, M.; Beekman, M. Strong HONO formation in a suburban site during snowy days. *Atmos. Environ.* **2015**, *116*, 155−158.

(13) Anderson, P. S.; Neff, W. D. Boundary layer physics over snow and ice. *Atmos. Chem. Phys.* **2008**, *8*, 3563−3582.

(14) Warren, S. G.; Brandt, R. E.; Grenfell, T. C. Visible and near ultraviolet absorption spectrum of ice from transmission of solar radiation into snow. *Appl. Opt.* **2006**, *45*, 5320−5334.

(15) Domine, F.; Shepson, P. B. Air-snow interactions and atmospheric chemistry. *Science* **2002**, *297*, 1506−1510.

(16) Grannas, A. M.; Jones, A. E.; Dibb, J.; Ammann, M.; Anastasio, C.; Beine, H. J.; Bergin, M.; Bottenheim, J.; Boxe, C. S.; Carver, G.; Chen, G.; Crawford, J. H.; Dominé, F.; Frey, M. M.; Guzmán, M. I.; Heard, D. E.; Helmig, D.; Hoffmann, M. R.; Honrath, R. E.; Huey, L. G.; Hutterli, M.; Jacobi, H. W.; Klán, P.; Lefer, B.; McConnell, J.; Plane, J.; Sander, R.; Savarino, J.; Shepson, P. B.; Simpson, W. R.; Sodeau, J. R.; von Glasow, R.; Weller, R.; Wolff, E. W.; Zhu, T. An overview of snow photochemistry: evidence, mechanisms and impacts. *Atmos. Chem. Phys.* **2007**, *7*, 4329−4373.

(17) Perner, D.; Platt, U. Detection of nitrous acid in the atmosphere by differential optical absorption. *Geophys. Res. Lett.* **1979**, *6*, 917−920.

(18) Spataro, F.; Ianniello, A. Sources of atmospheric nitrous acid: State of the science, current research needs, and future prospects. *J. Air Waste Manage. Assoc.* **2014**, *64* (11), 1232−1250.

(19) Zhou, X.; Beine, H. J.; Honrath, R. E.; Fuentes, J. D.; Simpson, W.; Shepson, P. B.; Bottenheim, J. W. Snowpack Photochemical production of HONO: a major source of OH in the Arctic boundary layer in springtime. *Geophys. Res. Lett.* **2001**, *28*, 4087−4090.

(20) Honrath, R. E.; Lu, Y.; Peterson, M. C.; Dibb, J. E.; Arsenault, M. A.; Cullen, N. J.; Steffen, K. Vertical fluxes of NOx, HONO and HNO3 above the snowpack at Summit, Greenland. *Atmos. Environ.* **2002**, *36*, 2629−2640.

(21) Amoroso, A.; Beine, H. J.; Sparapani, R.; Nardino, M.; Allegrini, I. Observation of coinciding Arctic boundary layer ozone depletion and snow surface emissions of nitrous acid. *Atmos. Environ.* **2006**, *40* (11), 1949−1956.

(22) Ye, C. X.; Zhou, X. L.; Pu, D.; Stutz, J.; Festa, J.; Spolaor, M.; Tsai, C.; Cantrell, C.; Mauldin, R. L.; Campos, T.; Weinheimer, A.; Hornbrook, R. S.; Apel, E. C.; Guenther, A.; Kaser, L.; Yuan, B.; Karl, T.; Haggerty, J.; Hall, S.; Ullmann, K.; Smith, J. N.; Ortega, J.; Knote,

DOI: 10.1021/acsearthspacechem.9b00023
ACS Earth Space Chem. XXXX, XXX, XXX−XXX

C. Rapid cycling of reactive nitrogen in the marine boundary layer. *Nature* **2016**, *532*, 489−491.
(23) Wang, L.; Wen, L.; Xu, C.; Chen, J.; Wang, X.; Yang, L.; Wang, W.; Yang, X.; Sui, X.; Yao, L.; Zhang, Q. HONO and its potential source particulate nitrite at an urban site in North China during the cold season. *Sci. Total Environ.* **2015**, *538*, 93−101.
(24) Kirchstetter, T.; Harley, R.; Littlejohn, D. Measurement of nitrous acid in motor vehicle exhaust. *Environ. Sci. Technol.* **1996**, *30*, 2843−2849.
(25) Kurtenbach, R.; Becker, K. H.; Gomes, J. A. G.; Kleffmann, J.; Lörzer, J. C.; Spittler, M.; Wiesen, P.; Ackermann, R.; Geyer, A.; Platt, U. Investigation of emissions and heterogeneous formation of HONO in a road traffic tunnel. *Atmos. Environ.* **2001**, *35*, 3385−3394.
(26) Li, Y. Q.; Schwab, J. J.; Demerjian, K. L. Fast time response measurements of gaseous nitrous acid using a tunable diode laser absorption spectrometer: Hono emission source from vehicle exhausts. *Geophys. Res. Lett.* **2008**, *35*, L04803.
(27) Nakashima, Y.; Kajii, Y. Determination of nitrous acid emission factors from a gasoline vehicle using a chassis dynamometer combined with incoherent broadband cavity-enhanced absorption spectroscopy. *Sci. Total Environ.* **2017**, *575*, 287−293.
(28) Pitts, J. N.; Biermann, H. W.; Tuazon, E. C.; Green, M.; Long, W. D.; Winer, A. M. Time-resolved identification and measurements of indoor air pollutants by spectroscopic techniques: gaseous nitric acid, methanol, formaldehyde, and formic acid. *JAPCA* **1989**, *39*, 1344−1347.
(29) Brauer, M.; Ryan, P. B.; Suh, H. H.; Koutrakis, P.; Spengler, J. D.; Leslie, N. P.; Billick, I. H. Measurements of nitrous acid inside two research houses. *Environ. Sci. Technol.* **1990**, *24*, 1521−1527.
(30) Wormhoudt, J.; Herndon, S. C.; Yelvington, P. E.; Miakelye, R. C.; Wey, C. Nitrogen oxide (NO/NO2/HONO) emissions measurements in aircraft exhausts. *J. Propul. Power* **2007**, *23* (5), 906−911.
(31) Bartolomei, V.; Gomez, A. E.; Wittmer, J.; Tlili, S.; Strekowski, R.; Temime-Roussel, B.; Quivet, E.; Wortham, H.; Zetzsch, C.; Kleffmann, J.; Gligorovski, S. Combustion processes as a source of high levels of indoor hydroxyl radicals through the photolysis of nitrous acid. *Environ. Sci. Technol.* **2015**, *49* (11), 6599−6607.
(32) Finlayson-Pitts, B. J.; Wingen, L. M.; Sumner, A. L.; Syomin, D.; Ramazan, K. A. The heterogeneous hydrolysis of NO2 in laboratory systems and in outdoor and indoor atmospheres - an integrated mechanism. *Phys. Chem. Chem. Phys.* **2003**, *5*, 223−242.
(33) Stemmler, K.; Ammann, M.; Donders, C.; Kleffmann, J.; George, C. Photosensitized reduction of nitrogen dioxide on humic acid as a source of nitrous acid. *Nature* **2006**, *440*, 195−198.
(34) Stemmler, K.; Ndour, M.; Elshorbany, Y.; Kleffmann, J.; D'Anna, B.; George, C.; Bohn, B.; Ammann, M. Light induced conversion of nitrogen dioxide into nitrous acid on submicron humic acid aerosol. *Atmos. Chem. Phys.* **2007**, *7*, 4237−4248.
(35) Ammann, M.; Kalberer, M.; Jost, D. T.; Tobler, L.; Rossler, E.; Piguet, D.; Gaggeler, H. W.; Baltensperger, U. Heterogeneous production of nitrous acid on soot in polluted air masses. *Nature* **1998**, *395*, 157−160.
(36) Ye, C.; Zhang, N.; Gao, H.; Zhou, X. Photolysis of particulate nitrate as a source of HONO and NOx. *Environ. Sci. Technol.* **2017**, *51*, 6849−6856.
(37) Ye, C.; Zhou, X.; Pu, D.; Stutz, J.; Festa, J.; Spolaor, M.; Tsai, C.; Cantrell, C.; Mauldin, R. L., III; Weinheimer, A.; Hornbrook, R. S.; Apel, E. C.; Guenther, A.; Kaser, L.; Yuan, B.; Karl, T.; Haggerty, J.; Hall, S.; Ullmann, K.; Smith, J.; Ortega, J. Tropospheric HONO distribution and chemistry in the southeastern US. *Atmos. Chem. Phys.* **2018**, *18*, 9107−9120.
(38) Kasibhatla, P.; Sherwen, T.; Evans, M. J.; Carpenter, L. J.; Reed, C.; Alexander, B.; Chen, Q.; Sulprizio, M. P.; Lee, J. D.; Read, K. A.; Bloss, W.; Crilley, L. R.; Keene, W. C.; Pszenny, A. A. P.; Hodzic, A. Global impact of nitrate photolysis in sea-salt aerosol on NOx, OH, and O3 in the marine boundary layer. *Atmos. Chem. Phys.* **2018**, *18*, 11185−11203.
(39) Zhang, N.; Zhou, X.; Shepson, P. B.; Gao, H.; Alaghmand, M.; Stirm, B. Aircraft measurement of HONO vertical profiles over a forested region. *Geophys. Res. Lett.* **2009**, *36*, L15820.
(40) Zhang, N.; Zhou, X.; Bertman, S.; Tang, D.; Alaghmand, M.; Shepson, P. B.; Carroll, M. A. Measurements of ambient HONO concentrations and vertical HONO flux above a northern Michigan forest canopy. *Atmos. Chem. Phys.* **2012**, *12*, 8285−8296.
(41) Wong, K. W.; Tsai, C.; Lefer, B.; Haman, C.; Grossberg, N.; Brune, W. H.; Ren, X.; Luke, W.; Stutz, J. Daytime HONO vertical gradients during SHARP 2009 in Houston, TX. *Atmos. Chem. Phys.* **2012**, *12*, 635−652.
(42) VandenBoer, T. C.; Brown, S. S.; Murphy, J. G.; Keene, W. C.; Young, C. J.; Pszenny, A. A. P.; Kim, S.; Warneke, C.; de Gouw, J. A.; Maben, J. R.; Wagner, N. L.; Riedel, T. P.; Thornton, J. A.; Wolfe, D. E.; Dubé, W. P.; Öztürk, F.; Brock, C. A.; Grossberg, N.; Lefer, B.; Lerner, B.; Middlebrook, A. M.; Roberts, J. M. Understanding the role of the ground surface in HONO vertical structure: High resolution vertical profiles during NACHTT-11. *J. Geophys. Res.-Atmos.* **2013**, *118*, 10155−10171.
(43) Tsai, C.; Spolaor, M.; Colosimo, S. F.; Pikelnaya, O.; Cheung, R.; Williams, E.; Gilman, J. B.; Lerner, B. M.; Zamora, R. J.; Warneke, C.; Roberts, J. M.; Ahmadov, R.; de Gouw, J.; Bates, T.; Quinn, P. K.; Stutz, J. Nitrous acid formation in a snow-free wintertime polluted rural area. *Atmos. Chem. Phys.* **2018**, *18*, 1977−1996.
(44) Zhou, X.; Civerolo, K.; Dai, H.; Huang, G.; Schwab, J.; Demerjian, K. Summertime nitrous acid chemistry in the atmospheric boundary layer at a rural site in New York State. *J. Geophys. Res.* **2002**, *107* (13), 1−11.
(45) Su, H.; Cheng, Y.; Oswald, R.; Behrendt, T.; Trebs, I.; Meixner, F. X.; reae, M. O.; Cheng, P.; Zhang, Y.; Pöschl, U. Soil nitrite as a source of atmospheric HONO and OH radicals. *Science* **2011**, *333*, 1616−1618.
(46) Oswald, R.; Behrendt, T.; Ermel, M.; Wu, D.; Su, H.; Cheng, Y.; Breuninger, C.; Moravek, A.; Mougin, E.; Delon, C.; Loubet, B.; Pommerening-RÖser, A.; SÖrgel, M.; PÖschl, U.; Hoffmann, T.; reae, M. O.; Meixner, F. X.; Trebs, I. HONO emissions from soil bacteria as a major source of atmospheric reactive nitrogen. *Science* **2013**, *341*, 1233−1235.
(47) Meusel, H.; Tamm, A.; Kuhn, U.; Wu, D.; Leifke, A. L.; Fiedler, S.; Ruckteschler, N.; Yordanova, P.; Lang-Yona, N.; Pöhlker, M.; Lelieveld, J.; Hoffmann, T.; Pöschl, U.; Su, H.; Weber, B.; Cheng, Y. Emission of nitrous acid from soil and biological soil crusts represents an important source of HONO in the remote atmosphere in Cyprus. *Atmos. Chem. Phys.* **2018**, *18*, 799−813.
(48) Amoroso, A.; Domine, F.; Esposito, G.; Morin, S.; Savarino, J.; Nardino, M.; Montagnoli, M.; Bonneville, J. M.; Clement, J. C.; Ianniello, A.; Beine, H. J. Microorganisms in dry polar snow are involved in the exchanges of reactive nitrogen species with the atmosphere. *Environ. Sci. Technol.* **2010**, *44*, 714−719.
(49) VandenBoer, T. C.; Young, C. J.; Talukdar, R. K.; Markovic, M. Z.; Brown, S. S.; Roberts, J. M.; Murphy, J. G. Nocturnal loss and daytime source of nitrous acid through reactive uptake and displacement. *Nat. Geosci.* **2015**, *8*, 55−60.
(50) Burkholder, J. B.; Sander, S. P.; Abbatt, J.; Barker, J. R.; Huie, R. E.; Kolb, C. E.; Kurylo, M. J.; Orkin, V. L.; Wilmouth, D. M.; Wine, P. H. Chemical Kinetics and Photochemical Data for Use in Atmospheric Studies, Evaluation No. 18. *JPL Publication 15−10*; Jet Propulsion Laboratory: Pasadena, 2015. http://jpldataeval.jpl.nasa.gov.
(51) Anglada, J. M.; Solé, A. The atmospheric oxidation of HONO by OH, Cl, and ClO radicals. *J. Phys. Chem. A* **2017**, *121* (51), 9698−9707.
(52) Harrison, R. M.; Peak, J. D.; Collins, G. M. Tropospheric cycle of nitrous acid. *J. Geophys. Res.-Atmos.* **1996**, *101*, 14429−14439.
(53) Park, J.-Y.; Lee, Y.-N. Solubility and decomposition kinetics of nitrous acid in aqueous solution. *J. Phys. Chem.* **1988**, *92*, 6294−6302.
(54) Riordan, E.; Minogue, N.; Healy, D.; O'Driscoll, P.; Sodeau, J. R. Spectroscopic and optimization modeling study of nitrous acid in aqueous solution. *J. Phys. Chem. A* **2005**, *109* (5), 779−786.

DOI: 10.1021/acsearthspacechem.9b00023
ACS Earth Space Chem. XXXX, XXX, XXX−XXX

(55) Liao, W.; Tan, D. 1-D Air-snowpack modeling of atmospheric nitrous acid at South Pole during ANTCI 2003. *Atmos. Chem. Phys.* **2008**, *8*, 7087−7099.
(56) VandenBoer, T. C.; Markovic, M. Z.; Sanders, J. E.; Ren, X.; Pusede, S. E.; Browne, E. C.; Cohen, R. C.; Zhang, L.; Thomas, J.; Brune, W. H.; Murphy, J. G. Evidence for a nitrous acid (HONO) reservoir at the ground surface in Bakersfield, CA, during CalNex 2010. *J. Geophys. Res. Atmos.* **2014**, *119*, 9093−9106.
(57) Lammel, G.; Perner, D. The atmospheric aerosol as a source of nitrous acid in the polluted atmosphere. *J. Aerosol Sci.* **1988**, *19* (7), 1199−1202.
(58) Li, S.-M. Particulate and snow nitrite in the spring arctic troposphere. *Atmos. Environ., Part A* **1993**, *27*, 2959−2967.
(59) Simon, P. K.; Dasgupta, P. K. Continuous automated measurement of gaseous nitrous and nitric acids and particulate nitrite and nitrate. *Environ. Sci. Technol.* **1995**, *29*, 1534−1541.
(60) Acker, K.; Möller, D.; Auel, R.; Wieprecht, W.; Kalass, D. Concentrations of nitrous acid, nitric acid, nitrite and nitrate in the gas and aerosol phase at a site in the emission zone during ESCOMPTE 2001 experiment. *Atmos. Res.* **2005**, *74*, 507−524.
(61) Acker, K.; Febo, A.; Trick, S.; Perrino, C.; Bruno, P.; Wiesen, P.; Moller, D.; Wieprecht, W.; Auel, R.; Giusto, M.; Geyer, A.; Platt, U.; Allegrini, I. Nitrous acid in the urban area of Rome. *Atmos. Environ.* **2006**, *40*, 3123−3133.
(62) Wang, Y.; Zhuang, G. S.; Tang, A. H.; Yuan, H.; Sun, Y. L.; Chen, S.; Zheng, A. H. The ion chemistry and the source of PM2.5 aerosol in Beijing. *Atmos. Environ.* **2005**, *39*, 3771−3784.
(63) Fisseha, R.; Dommen, J.; Gutzwiller, L.; Weingartner, E.; Gysel, M.; Emmenegger, C.; Kalberer, M.; Baltensperger, U. Seasonal and diurnal characteristics of water soluble inorganic compounds in the gas and aerosol phase in the Zurich area. *Atmos. Chem. Phys.* **2006**, *6*, 1895−1904.
(64) Kuprov, R.; Eatough, D. J.; Cruickshank, T.; Olson, N.; Cropper, P. M.; Hansen, J. C. Composition and secondary formation of fine particulate matter in the Salt Lake Valley: Winter 2009. *J. Air Waste Manage. Assoc.* **2014**, *64*, 957−969.
(65) Song, C. H.; Park, M. E.; Lee, E. J.; Lee, J. H.; Lee, B. K.; Lee, D. S.; Kim, J.; Han, J. S.; Moon, K. J.; Kondo, Y. Possible particulate nitrite formation and its atmospheric implications inferred from the observations in Seoul, Korea. *Atmos. Environ.* **2009**, *43*, 2168−2173.
(66) Dubowski, Y.; Colussi, A. J.; Boxe, C.; Hoffmann, M. R. Monotonic increase of nitrite yields in the photolysis of nitrate in ice and water between 238 and 294 K. *J. Phys. Chem. A* **2002**, *106*, 6967−6971.
(67) Becker, K. H.; Kleffmann, J.; Negri, R. M.; Wiesen, P. Solubility of nitrous acid (HONO) in ammonium sulphate solutions. *J. Chem. Soc. Faraday. Trans.* **1998**, *94*, 1583−1586.
(68) Donaldson, M. A.; Berke, A. E.; Raff, J. D. Uptake of gas phase nitrous acid onto boundary layer soil surfaces. *Environ. Sci. Technol.* **2014**, *48*, 375−383.
(69) Chu, L.; Anastasio, C. Temperature and wavelength dependence of nitrite photolysis in frozen and aqueous solutions. *Environ. Sci. Technol.* **2007**, *41*, 3626−3632.
(70) Naumov, S.; Mark, G.; Jarocki, A.; von Sonntag, C. The reactions of nitrite ion with ozone in aqueous solution − new experimental data and quantum-chemical considerations. *Ozone: Sci. Eng.* **2010**, *32* (6), 430−434.
(71) Jacobi, H. W.; Hilker, B. A mechanism for the photochemical transformation of nitrate in snow. *J. Photochem. Photobiol., A* **2007**, *185*, 371−382.
(72) Jacobi, H. W.; Kleffmann, J.; Villena, G.; Wiesen, P.; King, M.; France, J.; Anastasio, C.; Staebler, R. Role of nitrite in the photochemical formation of radicals in the snow. *Environ. Sci. Technol.* **2014**, *48* (1), 165−172.
(73) Zuo, Y.; Wang, C.; Van, T. Simultaneous determination of nitrite and nitrate in dew, rain, snow and lake water samples by ion-pair high-performance liquid chromatography. *Talanta* **2006**, *70* (2), 281−285.
(74) Chu, L.; Anastasio, C. Quantum yields of hydroxyl radical and nitrogen dioxide from the photolysis of nitrate on ice. *J. Phys. Chem. A* **2003**, *107*, 9594−9602.
(75) Boxe, C. S.; Saiz-Lopez, A. Multiphase modeling of nitrate photochemistry in the quasi-liquid layer (QLL): implications for NOx release from the Arctic and coastal Antarctic snowpack. *Atmos. Chem. Phys.* **2008**, *8*, 4855−4864.
(76) Warneck, P.; Wurzinger, C. Product quantum yields for the 305 nm photodecomposition of NO3- in aqueous-solution. *J. Phys. Chem.* **1988**, *92*, 6278−6283.
(77) Dubowski, Y.; Colussi, A. J.; Hoffmann, M. R. Nitrogen dioxide release in the 302 nm band photolysis of spray-frozen aqueous nitrate solutions: Atmospheric Implications. *J. Phys. Chem. A* **2001**, *105*, 4928−4932.
(78) Stanier, C.; Singh, A.; Adamski, W.; Baek, J.; Caughey, M.; Carmichael, G.; Edgerton, E.; Kenski, D.; Koerber, M.; Oleson, J.; Rohlf, T.; Lee, S. R.; Riemer, N.; Shaw, S.; Sousan, S.; Spak, S. N. Overview of the LADCO winter nitrate study: hourly ammonia, nitric acid and PM2.5 composition at an urban and rural site pair during PM2.5 episodes in the US Great Lakes region. *Atmos. Chem. Phys.* **2012**, *12*, 11037−11056.
(79) Cohen, L.; Helmig, D.; Neff, W.; Grachev, A.; Fairall, C. Boundary-layer dynamics and its influence on atmospheric chemistry at Summit, Greenland. *Atmos. Environ.* **2007**, *41* (24), 5044−5060.
(80) Seinfeld, J. H.; Pandis, S. N. *Atmospheric chemistry and physics: from air pollution to climate change*, 2nd ed.; John Wiley and Sons, Inc.: Hoboken, NJ, 2006.
(81) Markovic, M. Z.; VandenBoer, T. C.; Murphy, J. G. Characterization and optimization of an online system for the simultaneous measurement of atmospheric water-soluble constituents in the gas and particle phases. *J. Environ. Monit.* **2012**, *14*, 1872−1884.
(82) Markovic, M.; VandenBoer, T.; Baker, K.; Kelly, J.; Murphy, J. Measurements and modeling of the inorganic chemical composition of fine particulate matter and associated precursor gases in California's San Joaquin Valley during CalNex 2010. *J. Geophys. Res.-Atmos.* **2014**, *119*, 6853−6866.
(83) Clegg, S. L.; Brimblecombe, P.; Wexler, A. S. A thermodynamic model of the system H+ - NH4+ - SO42− - NO3− - H2O at tropospheric temperatures. *J. Phys. Chem. A* **1998**, *102*, 2137−2154.
(84) Murphy, J. G.; Gregoire, P. K.; Tevlin, A. G.; Wentworth, G. R.; Ellis, R. A.; Markovic, M. Z.; VandenBoer, T. C. Observational constraints on particle acidity using measurements and modelling of particles and gases. *Faraday Discuss.* **2017**, *200*, 379−395.
(85) Markvart, T.; Castalzer, L. *Practical handbook of photovoltaics: fundamentals and applications*; Elsevier, 2003.
(86) Kleinman, L.; Lee, Y.-N.; Springston, S. R.; Lee, J. H.; Nunnermacker, L.; Weinsten-Lloyd, J.; Zhou, X.; Newman, L. Peroxy radical concentration and ozone formation rate at a rural site in southeastern United States. *J. Geophys. Res.* **1995**, *100*, 7263−7273.
(87) Villena, G.; Wiesen, P.; Cantrell, C. A.; Flocke, F.; Fried, A.; Hall, S. R.; Hornbrook, R. S.; Knapp, D.; Kosciuch, E.; Mauldin, R. L., III; McGrath, J. A.; Montzka, D.; Richter, D.; Ullmann, K.; Walega, J.; Weibring, P.; Weinheimer, A.; Staebler, R. M.; Liao, J.; Huey, L. G.; Kleffman, J. Nitrous acid (HONO) during polar spring in Barrow, Alaska: a net source of OH radicals? *J. Geophys. Res.* **2011**, *116*, D00R07.
(88) Acker, K.; Möller, D.; Wieprecht, W.; Meixner, F. X.; Bohn, B.; Gilge, S.; Plass-Dülmer, C.; Berresheim, H. Strong daytime production of OH from HNO2 at a rural mountain site. *Geophys. Res. Lett.* **2006**, *33*, L02809.
(89) George, C.; Strekowski, R. S.; Kleffmann, J.; Stemmler, K.; Ammann, M. Photoenhanced uptake of gaseous NO2 on solid organic compounds: a photochemical source of HONO? *Faraday Discuss.* **2005**, *130*, 195−210.
(90) Stull, R. B. *An introduction to boundary layer meteorology*; Kluwer Academic Publishers: Dordrecht, 1988.
(91) Liao, W.; Tan, D. 1-D Air-snowpack modeling of atmospheric nitrous acid at South Pole during ANTCI 2003. *Atmos. Chem. Phys.* **2008**, *8*, 7087−7099.

DOI: 10.1021/acsearthspacechem.9b00023
ACS Earth Space Chem. XXXX, XXX, XXX−XXX

(92) Kolesar, K. R.; Mattson, C. N.; Peterson, P. K.; May, N. W.; Prendergast, R. K.; Pratt, K. A. Increases in wintertime PM2.5 sodium and chloride linked to snowfall and road salt application. *Atmos. Environ.* **2018**, *177*, 192−202.
(93) Kerbrat, M.; Huthwelker, T.; Gäggeler, H. W.; Ammann, M. Interaction of nitrous acid with polycrystalline ice: Adsorption on the surface and diffusion into the bulk. *J. Phys. Chem. C* **2010**, *114*, 2208−2219.
(94) Pinzer, B.; Kerbrat, M.; Huthwelker, T.; Gäggeler, H. W.; Schneebeli, M.; Ammann, M. Diffusion of NOx and HONO in snow: A laboratory study. *J. Geophys. Res.* **2010**, *115*, D03304.
(95) Crowley, J. N.; Ammann, M.; Cox, R. A.; Hynes, R. G.; Jenkin, M. E.; Mellouki, A.; Rossi, M. J.; Troe, J.; Wallington, T. J. Evaluated kinetic and photochemical data for atmospheric chemistry: Volume V − heterogeneous reactions on solid substrates. *Atmos. Chem. Phys.* **2010**, *10*, 9059−9223.
(96) Domine, F.; Taillandier, A.-S.; Simpson, W. R. A parameterization of the specific surface area of snow in models of snowpack evolution, based on 345 measurements. *J. Geophys. Res.* **2007**, *112*, F02031.
(97) Domine, F.; Albert, M.; Huthwelker, T.; Jacobi, H.-W.; Kokhanovsky, A. A.; Lehning, M.; Picard, G.; Simpson, W. R. Snow physics as relevant to snow photochemistry. *Atmos. Chem. Phys.* **2008**, *8*, 171−208.
(98) Bartels-Rausch, T.; Jacobi, H.-W.; Kahan, T. F.; Thomas, J. L.; Thomson, E. S.; Abbatt, J. P. D.; Ammann, M.; Blackford, J. R.; Bluhm, H.; Boxe, C.; Domine, F.; Frey, M. M.; Gladich, I.; Guzmán, M. I.; Heger, D.; Huthwelker, Th.; Klán, P.; Kuhs, W. F.; Kuo, M. H.; Maus, S.; Moussa, S. G.; McNeill, V. F.; Newberg, J. T.; Pettersson, J. B. C.; Roeselová, M.; Sodeau, J. R. A review of air−ice chemical and physical interactions (AICI): liquids, quasi-liquids, and solids in snow. *Atmos. Chem. Phys.* **2014**, *14*, 1587−1633.
(99) Malley, P.; Chakraborty, S.; Kahan, T. Physical characterization of frozen saltwater solutions using Raman microscopy. *ACS Earth Space Chem.* **2018**, *2* (7), 702−710.
(100) Kraus, A.; Hofzumahaus, A. Field measurements of atmospheric photolysis frequencies for O3, NO2, HCHO, CH3CHO, H2O2, and HONO by UV spectroradiometry. *J. Atmos. Chem.* **1998**, *31*, 161−180.
(101) Monks, P. S. Gas-phase radical chemistry in the troposphere. *Chem. Soc. Rev.* **2005**, *34* (4), 376−395.
(102) Sörgel, M.; Regelin, E.; Bozem, H.; Diesch, J.-M.; Drewnick, F.; Fischer, H.; Harder, H.; Held, A.; Hosaynali-Beygi, Z.; Martinez, M.; Zetzsch, C. Quantification of the unknown HONO daytime source and its relation to NO2. *Atmos. Chem. Phys.* **2011**, *11*, 10433−10447.
(103) Ryan, R. G.; Rhodes, S.; Tully, M.; Wilson, S.; Jones, N.; Frieß, U.; Schofield, R. Daytime HONO, NO2 and aerosol distributions from MAX-DOAS observations in Melbourne. *Atmos. Chem. Phys.* **2018**, *18*, 13969−13985.
(104) Reed, C.; Evans, M. J.; Crilley, L. R.; Bloss, W. J.; Sherwen, T.; Read, K. A.; Lee, J. D.; Carpenter, L. J. Evidence for renoxification in the tropical marine boundary layer. *Atmos. Chem. Phys.* **2017**, *17*, 4081−4092.
(105) Young, C. J.; Washenfelder, R. A.; Roberts, J. M.; Mielke, L. H.; Osthoff, H. D.; Tsai, C.; Pikelnaya, O.; Stutz, J.; Veres, P. R.; Cochran, A. K.; VandenBoer, T. C.; Flynn, J.; Grossberg, N.; Haman, C. L.; Lefer, B.; Stark, H.; Graus, M.; de Grouw, J.; Gilman, J. B.; Kuster, W. C.; Brown, S. S. Vertically resolved measurements of nighttime radical reservoirs in Los Angeles and their contribution to the urban radical budget. *Environ. Sci. Technol.* **2012**, *46*, 10965−10973.
(106) Edwards, P. M.; Brown, S. S.; Roberts, J. M.; Ahmadov, R.; Banta, R. M.; deGouw, J. A.; Dube, W. P.; Field, R. A.; Flynn, J. H.; Gilman, J. B.; Graus, M.; Helmig, D.; Koss, A.; Langford, A. O.; Lefer, B. L.; Lerner, B. M.; Li, R.; Li, S.-M.; McKeen, S. A.; Murphy, S. M.; Parrish, D. D.; Senff, C. J.; Soltis, J.; Stutz, J.; Sweeney, C.; Thompson, C. R.; Trainer, M. K.; Tsai, C.; Veres, P. R.; Washenfelder, R. A.; Warneke, C.; Wild, R. J.; Young, C. J.; Yuan, B.; Zamora, R. High winter ozone pollution from carbonyl photolysis in an oil and gas basin. *Nature* **2014**, *514*, 351−354.
(107) Zatko, M. C.; Erbland, J.; Savarino, J.; Geng, L.; Easley, L.; Schauer, A. J.; Bates, T. S.; Quinn, P.; Light, B.; Morison, D.; Osthoff, H. D.; Lyman, S.; Neff, W.; Yuan, B.; Alexander, B. The magnitude of the snow-sourced reactive nitrogen flux to the boundary layer in the Uintah Basin, Utah, USA. *Atmos. Chem. Phys.* **2016**, *16*, 13837−13851.
(108) Romer, P. S.; Wooldridge, P. J.; Crounse, J. D.; Kim, M. J.; Wennberg, P. O.; Dibb, J. E.; Blake, D. R.; Meinardi, S.; Brosius, A. L.; Thames, A. B.; Miller, D. O.; Brune, W. H.; Hall, S. R.; Ryerson, T. B.; Cohen, R. C. Constraints on aerosol nitrate photolysis as a potential source of HONO and NOx. *Environ. Sci. Technol.* **2018**, *52* (23), 13738−13746.
(109) Legrand, M.; Preunkert, S.; Frey, M.; Bartels-Rausch, Th.; Kukui, A.; King, M. D.; Savarino, J.; Kerbrat, M.; Jourdain, B. Large mixing ratios of atmospheric nitrous acid (HONO) at Concordia (East Antarctic Plateau) in summer: a strong source from surface snow? *Atmos. Chem. Phys.* **2014**, *14*, 9963−9976.
(110) Guimbaud, C.; Grannas, A. M.; Shepson, P. B.; Fuentes, J. D.; Boudries, H.; Bottenheim, J. W.; Domine, F.; Houdier, S.; Perrier, S.; Biesenthal, T. B.; Splawn, B. G. Snowpack processing of acetaldehyde and acetone in the Arctic atmospheric boundary layer. *Atmos. Environ.* **2002**, *36*, 2743−2752.
(111) Honrath, R. E.; Guo, S.; Peterson, M. C.; Dziobak, M. P.; Dibb, J. E.; Arsenault, M. A. Photochemical production of gas phase NOx from ice crystal NO3-. *J. Geophys. Res.* **2000**, *105*, 24183−24190.
(112) Honrath, R. E.; Peterson, M. C.; Dziobak, M. P.; Dibb, J. E.; Arsenault, M. A.; Green, S. A. Release of NOx from sunlight-irradiated midlatitude snow. *Geophys. Res. Lett.* **2000**, *27*, 2237−2240.
(113) Boxe, C. S.; Colussi, A. J.; Hoffmann, M. R.; Murphy, J. G.; Wooldridge, P. J.; Bertram, T. H.; Cohen, R. C. Photochemical production and release of gaseous NO2 from nitrate-doped water ice. *J. Phys. Chem. A* **2005**, *109* (38), 8520−8525.

DOI: 10.1021/acsearthspacechem.9b00023
ACS Earth Space Chem. XXXX, XXX, XXX−XXX